

Circuit-Theoretic Joint Parameter-State Estimation of Utility-Scale Photovoltaic, Battery, and Grid Systems

Peng Sang

The University of Vermont
peng.sang@uvm.edu

Amritanshu Pandey

The University of Vermont
amritanshu.pandey@uvm.edu

Abstract—Solar PV and battery storage systems have become integral to modern power grids. Therefore, bulk grid models in real-time operation must include their physical behavior accurately for analysis and optimization. AC state estimation is critical to building real-time bulk power systems models. However, current ACSE techniques do not include detailed physics and measurements for battery and PV systems. This results in sub-optimal estimation results and subsequent less accurate bulk grid models for real-time operation.

To address these challenges, we formulate a circuit-theoretic AC state estimator with accurate PV and battery systems physics and corresponding measurements. First, we propose an aggregated equivalent circuit model of the solar PV, battery, and traditional grid components. Next, we add measurements from PV and battery systems to the traditional measurement set to facilitate accurate estimation of the overall grid model. Finally, we develop a circuit-theoretic joint parameter-state estimation algorithm that can accurately estimate grid, PV, and battery system states and is robust against erroneous parameters. To demonstrate the efficacy of the proposed framework, we estimate the states of 10k node transmission networks with hundreds of battery+PV-tied systems. We compare the accuracy against the estimation of stand-alone grid, battery, and PV systems.

Keywords: Battery models, equivalent circuit modeling, joint parameter-state estimation, photovoltaic models, steady-state

NOMENCLATURE

General Symbols

\mathcal{P}	Set of circuit model parameters
\mathcal{P}_U	Set of unknown circuit model parameters
\mathcal{H}	Set of combined network constraints
\mathcal{Z}	Set of measurements
\mathcal{W}	Error covariance matrix
η_{inv}	Inverter efficiency (DC-AC)
η_{rec}	Rectifier efficiency (AC-DC)
$\hat{\mathcal{P}}_U$	Parameter estimates
N_s	Number of samples
N_c	Number of components

Grid Specific Symbols

\mathcal{N}	Set of all grid buses
\mathcal{N}_{ZI}	Set of zero-injection buses
\mathcal{M}	Set of grid measurement circuits (e.g., RTUs measuring injection power)
\mathcal{G}	Set of grid components without measurements (e.g., line, transformer, etc.)
\tilde{V}_k	Complex nodal voltage at bus k
V_k^r, V_k^i	Real/imaginary voltage at bus k
V_{kl}^r, V_{kl}^i	Real/imaginary voltage difference between bus k and l
$ V _k, \theta_k$	Voltage magnitude/angle at bus k
P_k, Q_k	Active/reactive power injection at bus k
P_k^G, Q_k^G	Real and reactive power injection of generator at bus k
P_k^L, Q_k^L	Real and reactive power injection of load at bus k
$ V _k^G$	Generator regulated voltage magnitude at bus k
$G_{z,k}, B_{z,k}$	Measurement feature transformation terms at bus k
$P_{k,z}, Q_{k,z}$	RTU injection measurements of real/reactive power at bus k
$ V _{k,z}$	RTU injection measurements of voltage magnitude at bus k
$\tilde{I}_k^G, \tilde{I}_k^L$	Generator and load complex current injection at bus k
n_k^r, n_k^i	Real and imaginary RTU measurement noise at bus k
G_{kl}, B_{kl}	Admittance terms between bus k and l
h_k^{Grid}	Set of current-voltage constraints for grid network physics at bus k

PV Specific Symbols

\mathcal{K}	Set of bulk grid-connected solar PV
---------------	-------------------------------------

R_S, R_{SH}	Series and shunt resistor of PV circuit
Z_{Load}	Grid equivalent impedance seen by the solar PV
V_{SH}	Voltage across shunt resistor in PV circuit, equal to open circuit voltage
$V_{PV}, V_{PV,z}$	Solar PV voltage at inverter terminal and its measurement
V_D	Diode voltage in solar PV circuit
$I_{PH}, I_{PH,z}$	PV photocurrent generation and measurement
I_D	Diode current in PV circuit
I_0	Saturation current of diode in PV circuit
$I_{PV}, I_{PV,z}$	Solar PV terminal current and its measurement
P_{PV}	PV DC injection power to inverter
$n_V^{PV}, n_I^{PV}, n_I^{PH}$	Solar PV voltage, current output, and photocurrent measurement noise terms
$w_I^{PV}, w_V^{PV}, w_{PH}^{PV}$	Weights for current, voltage, and photocurrent measurements for PV
h_k^{PV}	Current-voltage constraints for k^{th} PV circuit on the grid

Battery Specific Symbols

\mathcal{L}	Set of battery systems connected to bulk grid
V_{SoC}	Voltage representation of battery SOC, range between 0V to 1V for empty to full
V_{OC}	Battery open circuit voltage
$V_{Bt}, V_{Bt,z}$	Battery terminal voltage and its measurement
$I_{Bt}, I_{Bt,z}$	DC battery current and its measurement
C_{cap}	Battery equivalent capacitor
R_{SE}, R_{SD}	Series and self-discharge resistor of battery
h_k^{Bt}	Current-voltage constraints for the k^{th} battery
n_V^{Bt}, n_I^{Bt}	Battery terminal voltage and current measurement noise terms
w_I^{Bt}, w_V^{Bt}	Weights for current and voltage measurements for battery

I. INTRODUCTION

Motivation: Modern transmission networks now integrate emerging energy sources, such as utility-scale solar, battery

storage, and fuel cells, alongside traditional synchronous generation. Among these, solar PV and battery systems are experiencing the fastest growth in several US regions [1], and this trend is expected to continue. Unlike traditional generators, these sources show i) higher fluctuation in power output, ii) a wider range of control with power electronics, and iii) increased instrumentation through more measurements. In some areas, solar PV and battery resources now dominate daytime generation [2], providing essential services like carbon-free energy, peak shaving, and demand response. *Therefore, an accurate real-time model and parameter state estimates are necessary to support these applications.* However, gaps remain in the effectiveness of current estimation methods. Traditional state estimation (SE) relies on constant power PV and PQ models, using power measurements from remote terminal units (RTUs) to estimate the states of photovoltaic (PV) and battery systems. This approach simplifies the solar PV and battery model to a power source or a negative load and neglects critical internal states. For example, the state of charge (SoC) of a battery is critical to estimate when planning for grid services like peak shaving or demand response, as SoC reflects the current capacity of the battery storage system. PQ and PV models limit us to the Coulomb counting method when it comes to SoC estimation. A more detailed model can provide an estimated open circuit voltage (V_{OC}) to conduct open circuit voltage-based SoC estimation, thus allowing a hybrid estimation of SoC, that is, to estimate SoC with both the Coulomb counting method and open circuit voltage to calculate SoC to find the solution that can satisfy both conditions. Literature like [3] has shown that the hybrid method generally provides better SoC estimation than individual methods.

Similarly, for utility-scale solar PV systems, constant power source approximation limits the potential to expand the model to account for weather conditions, including irradiance temperature, and incorporate additional measurements from the solar PV systems. The utility-scale solar PV systems are generally well-equipped with sensors and communication infrastructure. This means the state variables in a utility-scale solar PV system can be measured directly by power electronic sensors and meteorological sensors, making it usually observable [4]. It is natural to make use of these measurements and enhance the redundancy level of our system.

However, it requires molding and parameterization of solar PV and battery storage systems to include measurements from them. The parameters generally are from spec sheets or lab test results, which represent either a batch or a type of equipment but do not accurately reflect exact parameters for the specific asset connected to the grid at a given time and condition and these inaccurate parameters will deteriorate the accuracy of state estimation (SE). *Therefore, in this work, we focus on estimating the states of battery and solar-connected transmission networks with circuit-based detailed models for solar PV and battery components and an assumption that certain model parameters may be erroneous.* The approach falls under the broad paradigm of joint parameter-state estimation.

To achieve this goal we build on prior works on equivalent circuit modeling and estimation [5], [6], and [7]. Both solar PV and battery systems can be characterized via equivalent circuit

This material is based upon work supported by the National Science Foundation through contract ECCS: 2330195 and the U.S. Department of Energy's Office of Energy Efficiency and Renewable Energy (EERE) under the Solar Energy Technologies Office Award Number DE-EE0010147. The views expressed herein do not necessarily represent the views of the U.S. Department of Energy or the United States Government.

models. Therefore, we include these circuit models within the broader equivalent circuit of the transmission network. We use the zeroth-order circuit model [8] to represent battery steady-state behavior and the single-diode circuit model [9] for the solar PV system. Further in our approach for joint parameter-state estimation, we consider additional measurements available from the battery and solar PV systems in addition to traditional remote terminal unit measurements.

State-of-art and limitations: Most current research on joint parameter-state estimation [4] and [10] focuses on transmission or distribution networks, with battery and solar PV systems often modeled like synchronous generation or negative load. Alternatively, they estimate [11]-[16] stand-alone battery and solar PV systems without coupling them to the grid.

The research is limited when considering the estimation and parameterization of combined solar PV, battery, and grid systems. For instance, [10] estimates PV fitting function parameters separately before applying them to the traditional SE formulation, while [4] introduces an augmented state estimation (ASE) approach using multiple measurements. Both works focus on estimating specific PV fitting function parameters rather than generic PV models.

Stand-alone PV system estimation research, such as [11], [12], and [13] solves optimization problems to estimate the PV states and parameters by minimizing the norm of the current residual to fit empirically obtained I-V curves. Stand-alone battery parameter estimation works [14], [15] minimize the residual norm between experimental measurements and model estimate. Other works like [16], minimize the time step integration of mismatch between voltage estimates and spec sheet voltage. These are all stand-alone techniques and do not include traditional grid measurements (e.g., from remote terminal units [RTUs]) to improve their estimation accuracy.

We find that key limitations of the state-of-the-art include the i) inability to represent the detailed physics of grid-tied battery and PV systems, ii) inability to include a wide array of measurements, and iii) inconsistent estimations of the states at the boundary of battery and PV system and the grid.

Insight of the problem: We will address these gaps by building a circuit-theoretic joint parameter estimation framework for transmission grid networks, including detailed models for utility solar PV and battery systems. In this approach, first, we will develop an aggregated circuit to model the physics of combined grid, utility-scale PV, and battery components. Next, in the aggregated circuit, we will replace or substitute the circuit element with its measurement equivalent where measurements are available. Finally, we will solve a large-scale optimization problem to obtain the system estimates. We will constrain the optimization problem by the physics of the measurement-based aggregated circuit, and in the objective, we will minimize noise terms in the measurement circuits. We will also model any potentially erroneous parameters as unknowns.

We anticipate several benefits from the proposed method in overcoming the mentioned limitations:

- **Generality to measurements:** The approach includes and uses a heterogeneous set of measurements from the

traditional grid meters and utility-scale battery and PV systems.

- **Solution consistency:** The estimates are consistent at the individual systems interconnect boundaries.
- **Robust against erroneous parameters:** The approach is robust to erroneous parameters in the system.

II. PRELIMINARIES

To build the joint circuit-based parameter-state estimation algorithm with grid-tied battery and solar PV systems, we describe the equivalent circuit models for grid, battery, and PV systems and state-of-the-art in circuit-theoretic state estimation.

A. Equivalent Circuit Modeling

In equivalent circuit modeling (ECM), we build equivalent circuits for individual grid components and aggregate them to represent the overall grid physics.

1) *Grid Modeling:* In ECM, circuit models for generator (PV), load (PQ), branch, transformer, and other grid components are derived from KCL-based current-voltage relationships. For example, consider node 2 in the 3-bus system in Fig.1 where the Kirchhoff current law (KCL) describes the nodal IV relationship:

$$I_{L,2}^r + V_{21}^r G_{21} - V_{21}^i B_{21} + V_{23}^r G_{23} - V_{23}^i B_{23} = 0 \quad (1)$$

$$I_{L,2}^i + V_{21}^i G_{21} + V_{21}^r B_{21} + V_{23}^i G_{23} + V_{23}^r B_{23} = 0 \quad (2)$$

The real and imaginary load currents in (1) and (2), are nonlinear functions of real and reactive power and complex voltages:

$$I_{L,2}^r = \frac{P_2 V_2^r + Q_2 V_2^i}{(V_2^r)^2 + (V_2^i)^2} \quad (3)$$

$$I_{L,2}^i = \frac{P_2 V_2^i - Q_2 V_2^r}{(V_2^r)^2 + (V_2^i)^2} \quad (4)$$

These relationships (and other similar relationships) can be directly mapped to circuit models. For instance, see the ECM representation of the power grid model in part (a) of Fig. 1 in part (b) of Fig. 1. Refer to [17], [18], and [19] for a comprehensive description of ECM for traditional grid components.

2) *Solar PV modeling:* To represent solar PV systems in ECM, we use the circuit-based single diode model (SDM) [20] shown in Fig. 2. SDM is widely used for its simplicity [21, 22, 23] and is sufficient to represent the amorphous silicon PV system [24] in comparison to more detailed double diode model (DDM).

In SDM, the photovoltaic, when not illuminated, behaves like a semiconductor diode whose voltage-current relationship is given by:

$$I_D = I_0 \left[\exp \left(\frac{qV_D}{nkT} \right) - 1 \right] \quad (5)$$

where the diode current (I_D) is calculated with Shockley diode equation (5). The voltage across the diode is noted as V_D . The k is the Boltzmann constant, and q is the electric charge for a single electron ($1.602e - 19$ C). I_0 represents the reverse

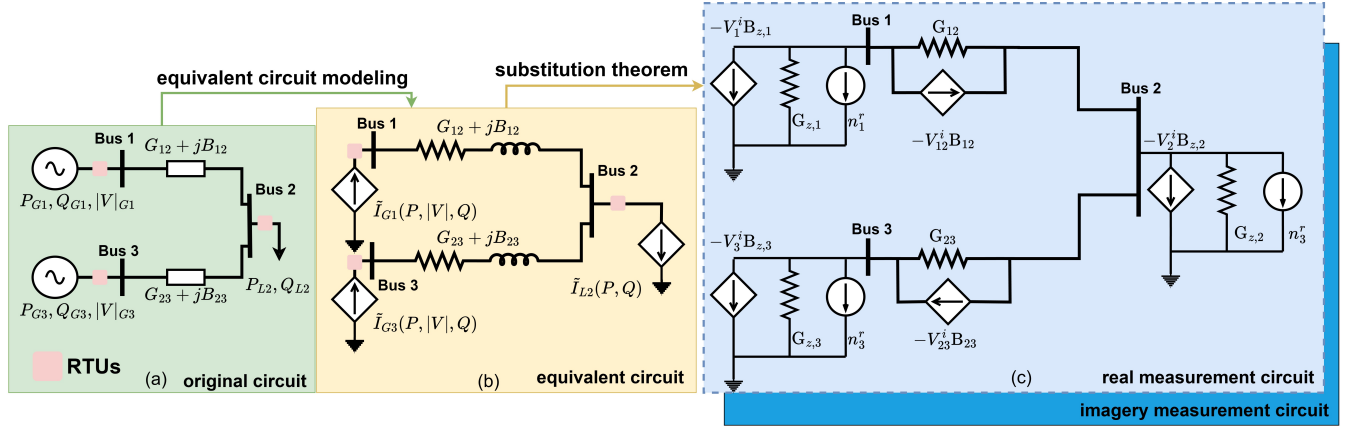


Fig. 1: (a)3-bus circuit example (b)with equivalent current source account for power injection (c)with RTUs represented as measurement circuits.

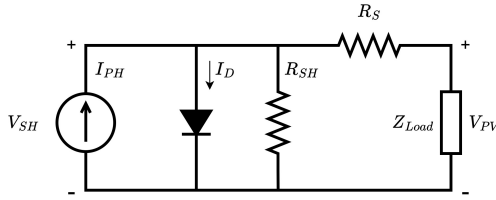


Fig. 2: Equivalent circuit of single diode model.

saturation current of the diode, and T is the cell temperature in Kelvin. n is the ideality factor of the diode, it is a factor that describes the diode quality and material of the diode (usually between 1 and 2). When n is unity, it represents an ideal diode; however, including leakage current pushes ideality factor n away from unity.

When illuminated, the diode provides a photocurrent (I_{PH}), modeled in SDM via a current source whose magnitude is a function of irradiance. This current divides into the diode current (I_D), leakage current (I_{SH}) through shunt resistance R_{SH} , and output current (I_{PV}). The losses in the interconnection junction box are modeled via series resistance (R_S). We can extend the SDM model to include PV system controls without loss of generality. For instance, [18] and [25] introduce circuit representation for maximum power point tracking (MPPT) and volt-var control, respectively.

3) *Battery modeling*: Equivalent circuits can also model the voltage-current characteristics of a battery. As the estimation and parameterization techniques in this paper focus on the *near* steady-state response of the aggregated grid, we neglect current-voltage transient behavior during charging and discharging and use a zeroth-order approximation of the battery circuit model in [8] to model voltage-current characteristics. The zeroth-order circuit is shown on the right of Fig. 3. The left of the figure represents the battery lifetime or the state of charge (SoC) dynamics. The battery lifetime subcircuit has the following components: a capacitor (C_{cap}) that is analogous to the rated capacity of the battery at full charge, a controlled current source that represents the current output (I_{Bt}), and a resistor (R_{SD}) connected in parallel to account for the battery's self-discharge.

The voltage across the capacitor (V_{SoC}) is analogous to the SoC of the battery and ranges between 0V and 1V, representing the fully discharged and fully charged state of the battery, respectively. The capacitance C_{cap} represents the ratio of the total charge stored in the battery as a function of V_{SoC} :

$$q_{cap} = C_{cap} V_{SoC} \quad (6)$$

With capacitor voltage V_{SoC} , and stored charge q_{cap} , the rate of change of q_{cap} is given by:

$$I_C = C_{cap} \frac{dV_{SoC}}{dt} \quad (7)$$

In the integral form, it can be written as:

$$V_{SoC,t} - V_{SoC,0} = \frac{1}{C_{cap}} \int_0^t I_C(t) dt \quad (8)$$

and the total charge transfer for time ranging from $t \rightarrow \tau$ in terms of ampere-hours is given by:

$$q_{cap,t} - q_{cap,0} = \int_0^\tau I_C(t) dt = - \int_0^\tau I_{Bt}(t) dt \quad (9)$$

The KCL-based relationship between the battery current I_{Bt} , self-discharge current (I_{SD}), capacitor current (I_C):

$$I_{SD} + I_C + I_{Bt} = 0 \quad (10)$$

By representing I_C and I_{SD} as functions of V_{SoC} we get the final form in (11):

$$\frac{V_{SoC}}{R_{SD}} + C_{cap} \frac{dV_{SoC}}{dt} + I_{Bt} = 0 \quad (11)$$

The right half of Fig.3 depicts the voltage-current characteristics of the battery. It has the following components: a voltage-controlled voltage source (V_{OC}), a series resistor (R_{SE}), and a controlled current source to represent current output (I_{Bt}) during constant power charge/discharge. We model the open circuit voltage as a fitted linear function of SoC (V_{OC}) with two fitted parameters a and b :

$$V_{SoC} = a + bV_{OC} \quad (12)$$

The terminal voltage of the battery (V_{Bt}) is given by Kirchhoff voltage law (KVL):

$$-V_{OC} + I_{Bt}R_{SE} + V_{Bt} = 0 \quad (13)$$

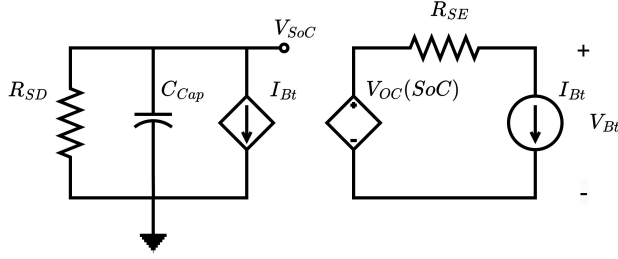


Fig. 3: Equivalent circuit of 0th order battery model.

4) *Inverter modeling*: The power converter bridges the DC battery and solar PV systems to the AC grid. The power transfer efficiency between the AC and DC systems is a function of operating power. For the estimation problem, we model the inverter efficiency with curve-fitted efficiency functions. We also assume the unity power factor for solar PV systems operation [18], thus for a PV at bus k :

$$P_k = \eta_{inv} P_{PV} \quad (14)$$

$$Q_k = Q_{PV} = 0 \quad (15)$$

In (14), the inverter efficiency is a function of solar PV power output, $\eta_{inv} = f^D(P_{PV})$ [26].

For this paper, akin to PV systems, we assume a unity power factor control for battery systems during discharge and inverter efficiency is given by $\eta_{inv} = f^D(P_{Bt})$. We assume the maximum charging efficiency is lower than the discharging efficiency for the battery per inverter spec sheet. Therefore, for charging efficiency, we use a separate fitted function $\eta_{rec} = f^C(P_{AC})$. For a battery connecting bus k , the equation is $\eta_{rec} = f^C(P_k)$. For both charging and discharging and inversion for PV systems, we chose the truncated sigmoid function to fit inverter curves for efficiency functions [26]. The function has following form:

$$\eta_{inv/rec} = \sigma(P) = \frac{M}{1 + e^{-\gamma P}} \quad (16)$$

During curve fitting to mimic the efficiency function, we estimate parameters M and γ with data from the inverter datasheet. P is positive in this setup thus we are using the positive part of the sigmoid function as shown in Fig. 4.

B. Circuit-theoretic State Estimation (*ckt-SE*)

In this paper, we build a method to estimate the grid states (including battery SOC and solar output) with many utility-sized battery and PV systems. We build the foundation of our work on existing circuit-theoretic grid estimation techniques in [5], [7], which introduce a convex circuit-based AC state estimation, termed **ckt-SE**. **ckt-SE** defines relationships between network physics and measurements via affine constraints in the current-voltage (IV) framework. As an initial step, in **ckt-SE**, we replace any equivalent circuit downstream of a measurement with a measurement circuit following the substitution theorem. However, as grid measurements are noisy, measurement circuits must include noise terms to satisfy KCL and KVL. Finally, to estimate grid states, **ckt-SE** minimizes the norm of the noise terms in the measurement circuit subject

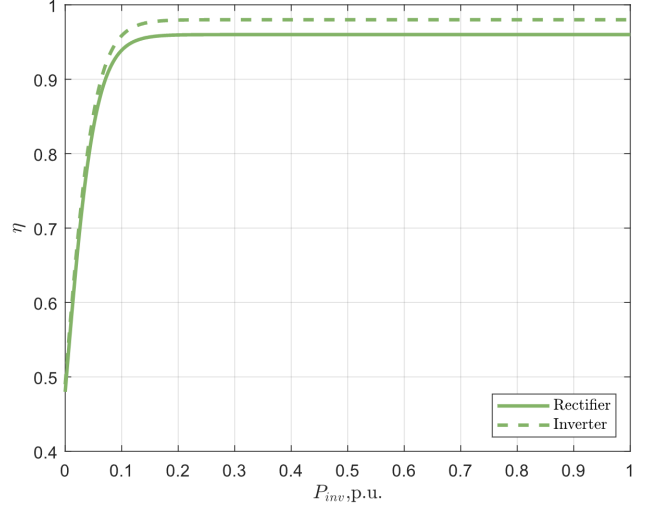


Fig. 4: Sigmoid efficiency curve used in this work.

to KCL and KVL-based grid constraints. We illustrate the idea of measurement circuits in Fig. 1 wherein the transition from Fig. 1(b) to Fig. 1(c) shows the use of measurement circuits. For instance, consider the node 2 load bus again in the 3-bus example. The bus has a remote terminal unit (RTU), which measures the real and reactive power consumption of the load ($P_{z,2}, Q_{z,2}$) and voltage magnitude ($|V|_{z,2}$) at the node. The nonlinear relationships between power and voltage-current behavior are non-affine, thus causing limitations like convergence issues.

To establish affine AC relationships and construct the measurement circuit for RTU measuring load parameters, these works ([5], [7], [18], and [6]) rely on feature transformation (17) that converts power and voltage measurements P_z , Q_z , and $|V|_z$ into conductance and susceptance (G_z , B_z) circuit elements. This feature transform can reduce three-dimensional measurements to two dimensions:

$$G_{z,2} = \frac{P_{z,2}}{(|V|_{z,2})^2}; \quad B_{z,2} = \frac{Q_{z,2}}{(|V|_{z,2})^2} \quad (17)$$

With the transformation, the nodal network constraints (or the measurement functions) at each bus are affine. For example, the injection currents I_{L2} at bus 2 are affine functions of unknown voltages:

$$I_{L2}^r = G_{z,2} V_2^r - B_{z,2} V_2^i + n_2^r \quad (18)$$

$$I_{L2}^i = G_{z,2} V_2^i + B_{z,2} V_2^r + n_2^i \quad (19)$$

In addition to the transformed measurements, equation (18) and (19) also include noise terms (n_2^r and n_2^i) to account for errors in power and voltage measurements.

Similarly, the approach also models other grid components with equivalent circuits. The works [5], [7] describe the creation of these circuits in length. Subsequently, it applies the substitution theorem to replace any measured circuit elements with a measurement circuit, as shown in Fig. 1(c). The approach then estimates the grid states by minimizing the norm of the noise terms in the measurement circuits subject to the constraints enforced by KCL equations at all buses

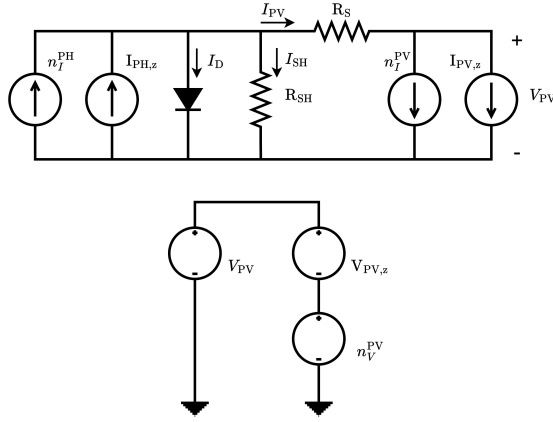


Fig. 5: Equivalent circuit of the PV system including measurements.

$h^{grid}(V, n)$. [6] further extends this framework to account for certain unknown parameters.

While robust and provably convex, this method does not include detailed circuit-based models for battery or solar PV systems or incorporate their corresponding measurements. The current approach is limited to RTU and PMU measurements only. The method also does not account for erroneous parameters. [6] considers erroneous parameters but is still limited to traditional grid parameters like line conductance and susceptance.

III. CIRCUIT-THEORETIC ESTIMATION OF COMBINED GRID, UTILITY-SCALE PV AND BATTERY SYSTEMS

Section II-A discussed the equivalent circuit models for grid, battery, and PV systems. Section II-B discussed the circuit-theoretic state-estimation approach, which includes measurements within the grid circuit model. Section III-A will build measurement circuits for grid-tied battery and PV systems and, subsequently, Section III-B will formulate the circuit-theoretic estimation problem **ckt-SE^{Re}** for bulk grid components, including battery and PV systems, as an optimization problem. The physics (defined by Kirchhoff's Laws) of the aggregated grid circuit, including measurement circuits, will define the constraint set of the **ckt-SE^{Re}** optimization problem. The minimization of measurement noise terms in the measurement circuits will serve as the objective of the estimation problem.

A. Measurement Circuits for PV and Battery

Section II-B (also [7] and [5]) describes the inclusion of RTU and PMU measurements into circuit-based estimation framework. Here, we derive circuits and corresponding equations for the inclusion of solar PV and battery measurements in the circuit-based framework.

1) *Solar PV measurement circuits*: We consider the following measurements for the solar PV systems: DC current ($I_{PV,z}$) and DC voltage ($V_{PV,z}$) at the inverter input terminal from meters at the inverter. We also calculate photocurrent ($I_{PH,z}$) from processed solar irradiance $S_{I,z}$ and ambient temperature $T_{amb,z}$ data from weather station, making it a *pseudo measurement* of I_{PH} [26], [27]. Note that all measurements represent

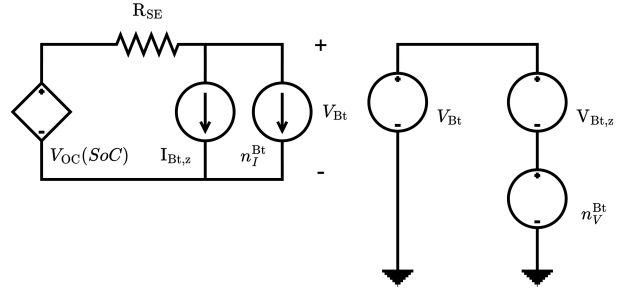


Fig. 6: Equivalent circuit of the battery system including measurements.

the aggregate contribution of panels that feed a single inverter. We model the measurement noise for DC terminal current, DC terminal voltage, and photocurrent with the following random variables: n_V^{PV} , n_I^{PV} , n_I^{PH} , respectively, and we assume Gaussian distribution for all.

To include measurements in the circuits framework, we use the substitution theorem to replace any measured component in the circuit with its corresponding measurements. Based on the PV system circuit in Fig. 2 this yields a new equivalent circuit, as shown in Fig. 5, which incorporates these measurements.

To represent the physics of the measurement-laden PV system circuit, we include the following KCL-based measurement functions:

$$-I_{PH,z} - n_I^{PH} + I_D + I_{SH} + I_{PV} = 0 \quad (20)$$

$$-I_{PV} + I_{PV,z} + n_I^{PV} = 0 \quad (21)$$

Now we represent all currents as functions of node voltages and noise variables. The current equations for shunt and series resistors are functions of voltage states:

$$I_{SH} = \frac{V_{SH}}{R_{SH}} \quad (22)$$

$$I_{PV} = \frac{V_{SH} - V_{PV}}{R_S} \quad (23)$$

For diode current, we set $nKT \rightarrow a$ in (24) to simplify (5) as they are all constants:

$$I_D = I_0 [e^{(V_{SH}/a)} - 1] \quad (24)$$

We use KVL to include the measurement function for DC voltage measurement:

$$-V_{PV} + V_{PV,z} + n_V^{PV} = 0 \quad (25)$$

In the estimation problem in Section III-B, we include the following relationships in (20) - (25) as constraints for each PV system.

2) *Battery Measurement Circuits*: For battery, we consider the following measurements: DC current ($I_{Bt,z}$) and DC voltage ($V_{Bt,z}$) at the inverter input terminal from the meter embedded in the inverter. Note that all measurements represent the aggregate contribution of battery cells and modules that feed a single inverter. We model the measurement noise with random variables (n_I^{Bt} , n_V^{Bt}) and assume Gaussian distribution for the noise terms.

Like PV systems, we use the substitution theorem to replace the measured components in the battery circuit with corresponding measurement-based sub-circuits. With these changes,

Fig.3 yields a measurement-based equivalent circuit, as shown in Fig.6. For measurement functions of the battery circuit, we include a KCL with DC battery current measurement and noise.

$$-I_{Bt} + I_{Bt,z} + n_I^{Bt} = 0 \quad (26)$$

$$\frac{V_{Bt} - V_{OC}}{R_S} + I_{Bt} = 0 \quad (27)$$

The KVL models the measurement function for DC voltage measurement:

$$-V_{Bt} + V_{Bt,z} + n_V^{Bt} = 0 \quad (28)$$

In general, SoC is hard to directly measure when the system is operating [8]. However, we can estimate SOC with different methods, as introduced in [28]. We estimate V_{SoC} with a linear fitted function mapping estimated V_{OC} to estimate V_{SoC} of the battery, and we also apply the Coulomb counting method to robustify the estimate further. The linear function is:

$$f_{voc}(V_{SoC}) : V_{OC}(t) = a + bV_{SoC}(t) \quad (29)$$

for any time step t . While the linear function describes the mapping between V_{SoC} and V_{OC} well in a certain range (SoC within 20%-80%), it is unsuitable for low and high SoC scenario modeling as the relationship gets nonlinear and (29) should be replaced by a nonlinear fitted equation.

We also know the relationship between battery current measurement and V_{SoC} , given by Kirchoff's current law (assuming very large R_{SD}):

$$I_{Bt,z} + n_I^{Bt} + C_{cap} \frac{dV_{SoC}}{dt} = 0 \quad (30)$$

To include this relation in the algebraic constraint set, we apply Trapezoidal approximation, substituting $I_{Bt,z}$ from (26):

$$V_{SoC}(t) - V_{SoC}(t - \Delta t) = -\frac{\Delta t}{2C_{cap}} (I_{Bt}(t) + I_{Bt}(t - \Delta t)) \quad (31)$$

Note that we know $(V_{SoC}(t - \Delta t), V_{OC}(t - \Delta t))$ from the prior estimation results or the initial condition. Next, we represent V_{SoC} as a function of V_{OC} :

$$\frac{V_{OC}(t) - V_{OC}(t - \Delta t)}{b} = -\frac{\Delta t}{2C_{cap}} (I_{Bt}(t) + I_{Bt}(t - \Delta t)) \quad (32)$$

Finally, substituting I_{Bt} with (27), we get:

$$\begin{aligned} & \frac{V_{OC}(t) - V_{OC}(t - \Delta t)}{b} = \\ & -\frac{\Delta t}{2C_{cap}} \left(\frac{V_{OC}(t) - V_{Bt}(t)}{R_S} - \frac{V_{OC}(t - \Delta t) - V_{Bt}(t - \Delta t)}{R_S} \right) \end{aligned} \quad (33)$$

Now, we include (33) in the battery constraint set to estimate V_{SoC} accurately.

B. Model Assembly

In this section, we interconnect and aggregate the equivalent circuits in Sections II-A and III-A to define the estimation problem's constraint set. The interconnected circuit includes both measurement circuits and those without measurement devices (e.g., zero-injection nodes).

Remark 1: To implement the constraint set of the estimation problem, we iterate through the equivalent circuit of each component and add Kirchoff-based network laws into the constraint set. The measurement information is embedded within the equivalent circuits.

As an example, consider the 3-bus example in Fig. 7. An inverter-connected battery system (green box) is connected to Bus 1 of the grid model (blue box), and an inverter-connected solar PV facility (yellow box) is connected to Bus 3 of the grid model. A load is connected to the Bus 2 of the grid.

To run an estimation study, we replace the measured components in Fig. 7 [top] with measurement-based equivalent circuits from Section III-A (see Fig. 7 [bottom]). We connect them together as shown in the dashed boxes in Fig. 7. We then write the IV relationships for each component in the aggregated circuit to describe the measurement functions or the constraint set for the estimation problem.

C. Circuit-based State Estimation as an Optimization

Forming optimization problem: Next, we formulate the optimization routines for the estimation problem. We formulate two sets of optimizations: i) *stand-alone* grid, battery, and PV system estimation routines, where each system independently models and estimates its states and ii) *combined* optimization routine, where grid, PV, and battery systems are modeled and estimated together.

1. Stand-alone Estimation Routines

Stand-alone grid formulation: The stand-alone grid estimation is introduced in Section II-B. The optimization minimizes noise realization in RTU measurements subject to grid network constraints:

$$\text{ckt-SE} : \sum_{m \in \mathcal{M}} f_m^{\text{Grid}}(n) \quad (34a)$$

subject to:

$$h_i^{\text{Grid}}(V, n) = 0 \quad \forall i \in \mathcal{N} \setminus \mathcal{N}_{ZI} \quad (34b)$$

$$h_i^{\text{Grid}}(V) = 0 \quad \forall i \in \mathcal{N}_{ZI} \quad (34c)$$

See [7],[5], and [6] to learn construction of objective function $f^{\text{Grid}}(n)$ and constraint set (34c) and (34b) for injection and zero injection nodes.

Stand-alone PV formulation: For stand-alone PV estimation, we minimize the weighted-noise realizations from PV system measurements: output DC current $I_{PV,z}$ and voltage $(V_{PV,z})$, and photocurrent $(I_{PH,z})$. The problem formulation is as follows:

$$\text{PV-SE} : \min_{V,n} f^{\text{PV}}(n) \quad (35a)$$

subject to:

$$h^{\text{PV}}(V, n) = 0 \quad (35b)$$

the constraint (35b) includes PV system's circuit's IV-relationships, described in (20) - (25) and the objective has the following form:

$$\begin{aligned} f^{\text{PV}}(n) = \min_{V,n} & \left(w_I^{\text{PV}} (n_I^{\text{PV}})^2 + w_V^{\text{PV}} (n_V^{\text{PV}})^2 \right. \\ & \left. + w_I^{\text{PH}} (n_I^{\text{PH}})^2 \right) \end{aligned} \quad (35c)$$

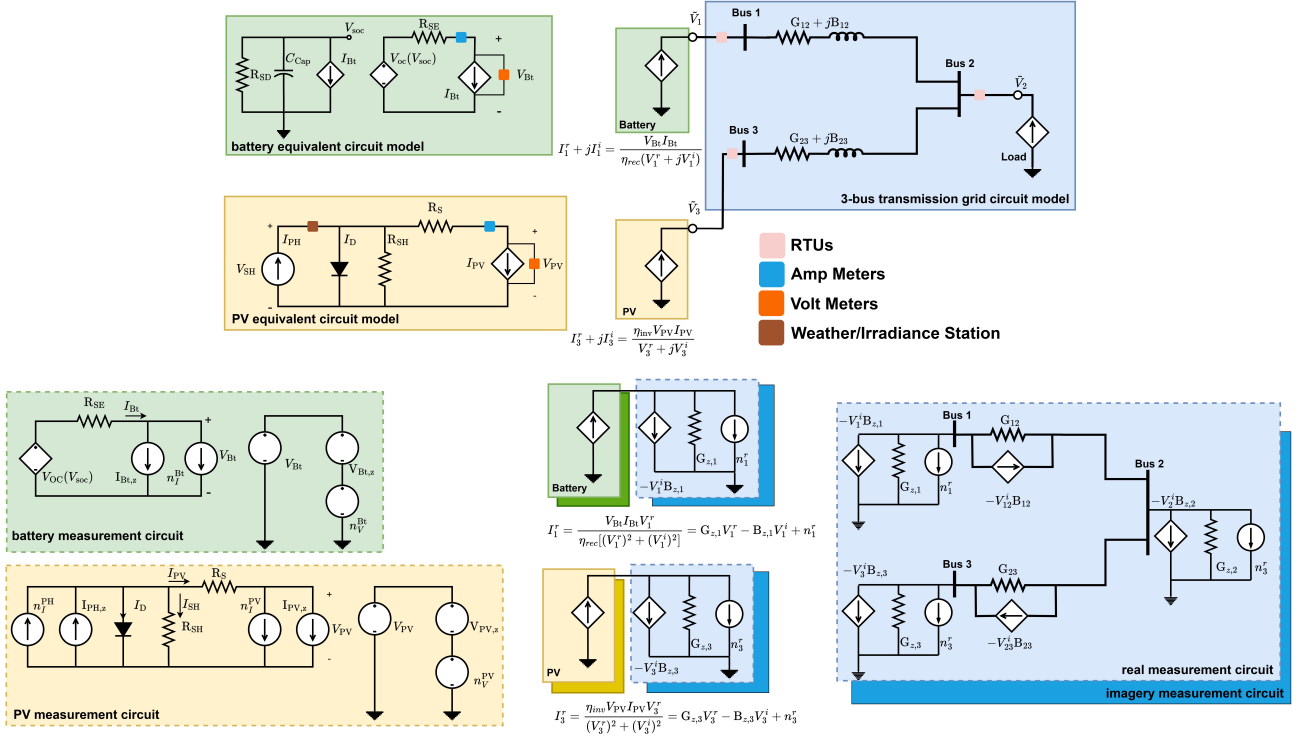


Fig. 7: This figure shows the combined 3-bus circuit example when the battery charges from the grid and the PV discharges to the grid. The upper half of the graph is ECM while the lower half is the measurement circuit.

In (35c), the weight (w) accounts for the spread in measurement accuracy and for measurement i , w_i is defined by the inverse of the measurement distribution variance σ_i^{-2} .

Stand-alone battery formulation: For stand-alone battery system estimation, we estimate the battery states, including SoC, given DC output voltage ($V_{Bt,z}$) and current ($I_{Bt,z}$) measurements:

$$\text{Bt-SE} : \min_{V,n} f^{\text{Bt}}(n) \quad (36a)$$

subject to:

$$h^{\text{Bt}}(V,n) = 0 \quad (36b)$$

(36b) includes constraints from (27) to (30) that describe the measurement functions for the battery. The objective is given in (36c), minimizing the weighted noise realizations in the battery measurements:

$$f^{\text{Bt}}(n) = \min_{V,n} \left(w_I^{\text{Bt}} (n_I^{\text{Bt}})^2 + w_V^{\text{Bt}} (n_V^{\text{Bt}})^2 \right) \quad (36c)$$

Overall, the stand-alone routines are easier to scale up as states for each system are estimated independently. However, the results of each subcircuit are not guaranteed to be consistent at the boundaries, and the impact of bad-data is significant in the estimate quality. Therefore, we formulate the estimation routine for combined PV, battery, and grid systems to address these challenges.

2. Combined Estimation Framework: **ckt-SE^{Re}**

Instead of estimating the states of solar PV or battery subsystems independently from the grid, in the combined formulation, we couple the utility-scale battery and PV systems with the bulk grid model, and we perform estimation on the coupled

model. We term this formulation: **ckt-SE^{Re}**. To couple the systems, we aggregate the equivalent circuits for PV, battery, and grid components in Section III-A and introduce a new set of coupling constraints that reconcile the physics at the point of interconnection (POI). The coupling constraints enforce the power balance between the solar PV and battery and grid subsystems. Inverters couple the various subsystems, and the behavior is dependent on the choice of control settings. For solar PV subsystems, we assume MPPT output. For battery subsystems, we assume constant PQ discharge or charge cycle based on an external dispatch schedule. For this work, we also assume unity power factor operation of the inverters and therefore reactive power transfer between the subsystems is assumed zero.

The grid circuit has both real and imaginary components. The AC power is obtained from complex voltage and current product. Subsequently, for solar PV at bus b , and MPPT control at unity power factor:

$$h^{\text{inv}} : \begin{cases} \eta_{inv} I_{PV} V_{PV} - (V_b^r I_b^r + V_b^i I_b^i) = 0 \\ V_b^i I_b^r - V_b^r I_b^i = 0 \end{cases} \quad (37)$$

For battery system at bus d , the constant power relationship is given by:

$$h^{\text{inv}} : \begin{cases} \eta_{inv} I_{Bt} V_{Bt} - (V_d^r I_d^r + V_d^i I_d^i) = 0, & \text{if discharging} \\ I_{Bt} V_{Bt} - \eta_{rec} (V_d^r I_d^r + V_d^i I_d^i) = 0, & \text{if charging} \\ V_d^i I_d^r - V_d^r I_d^i = 0 \end{cases} \quad (38)$$

In the combined setup, these inverter equations couple the stand-alone voltage and current measurements with RTU measurements recorded at the sub-station (see (17), (18) and (19)). Note that both rectification (charge) and inversion (discharging) efficiencies are functions of operating power and are discussed in the inverter section II-A4. As solar PV does not consume power from the grid, we only consider injecting power balance (37). The coupling constraints for battery (38) considers both charging and discharging scenarios. For example, Fig. 7 shows the battery charging with (38) and PV discharging with (37) at bus 1 and bus 3, respectively.

We summarize the combined state estimation of PV, battery and grid systems in (39):

$$\mathbf{ckt-SE}^{\text{Re}} : \min_{V,n} f(n) \quad (39a)$$

subject to:

$$h_i^{\text{Grid}}(V, n) = 0 \quad \forall i \in \mathcal{N} \setminus \mathcal{N}_{ZI} \quad (39b)$$

$$h_i^{\text{Grid}}(V) = 0 \quad \forall i \in \mathcal{N}_{ZI} \quad (39c)$$

$$h_k^{\text{PV}}(V, n) = 0 \quad \forall k \in \mathcal{K} \quad (39d)$$

$$h_l^{\text{Bt}}(V, n) = 0 \quad \forall l \in \mathcal{L} \quad (39e)$$

$$h_i^{\text{inv}}(V) = 0 \quad \forall i \in \mathcal{K} \cup \mathcal{L} \quad (39f)$$

where, i is a grid bus index and k and l are PV and battery circuit-index. \mathcal{K} and \mathcal{L} are sets of solar PV and battery systems, respectively. $\mathcal{N} \setminus \mathcal{N}_{ZI}$ is a set of grid buses with RTU on it, and \mathcal{N}_{ZI} are unmeasured zero-injection buses. The constraints for grid, battery, and solar PV are identical to the stand-alone method (35b) and (36b). Except, in the combined approach, we include the extra inverter-based coupling constraints for PV and battery systems.

The norm-2 minimization in objective has the following form:

$$f(n) = \min_{V,n} \left(\sum_{k \in \mathcal{K}} f_k^{\text{PV}}(n) + \sum_{l \in \mathcal{L}} f_l^{\text{Bt}}(n) + \sum_{m \in \mathcal{M}} f_m^{\text{Grid}}(n) \right) \quad (39g)$$

3. Include erroneous parameters: $\mathbf{ckt-PSE}^{\text{Re}}$

In the combined $\mathbf{ckt-SE}^{\text{Re}}$ and stand-alone algorithms, the circuit parameters (\mathcal{P}) like R_S, R_{SH} for solar PV circuits and R_{SE} for battery circuits, are considered known. However, in many real-world instances, these parameters might be erroneous. For solar PV systems, R_S can deviate from the fact sheet number due to the adjustments on wiring, replacement or aging of cable, and other reasons such as human error during data input. For battery systems, the internal resistance changes with the battery system's age and the cell's temperature. To address this, we modify our $\mathbf{ckt-SE}^{\text{Re}}$ to include erroneous parameters. In the algorithm, we replace the erroneous parameters (\mathcal{P}_U) as unknown variables and solve them within the optimization problem. We term the algorithm with this adjustment as $\mathbf{ckt-PSE}^{\text{Re}}$ to differentiate from $\mathbf{ckt-SE}^{\text{Re}}$ algorithm without erroneous parameters. We summarize the $\mathbf{ckt-PSE}^{\text{Re}}$ algorithm in Algorithm 1.

Algorithm 1 $\mathbf{ckt-PSE}^{\text{Re}}$

```

1: Input:  $\mathcal{P}, \mathcal{P}_U, \mathcal{Z}, \mathcal{W}, \mathcal{K}, \mathcal{L}, \mathcal{M}, \mathcal{G}$ 
2: Set:  $\mathcal{H} = \phi$  (empty constraint set),  $f(n) = 0$  (obj. fcn)


---


3: Step 1: Iterate through components with meas ( $\mathcal{K} \cup \mathcal{L} \cup \mathcal{M}$ )
   and add terms to the constraint set  $\mathcal{H}$ :
4: for  $m \in \mathcal{K} \cup \mathcal{L} \cup \mathcal{M}$  do   ▷ for every measurement ckt.
5:    $\mathcal{Z}_m \leftarrow \mathcal{Z}$            ▷ get ckt. meas from meas set
6:    $\mathcal{P}_m \leftarrow \mathcal{P}$          ▷ get ckt params from param set
7:   Add measurement func. to the constraint set:
8:   if  $\exists \mathcal{P}_m \in \mathcal{P}_U$  then     ▷ If parameter unknown
9:      $\mathcal{H} \leftarrow \mathcal{H} \cup h_m(V, n, \mathcal{P}_m)$ 
10:  else
11:     $\mathcal{H} \leftarrow \mathcal{H} \cup h_m(V, n)$ 
12:  end if
13:  Form component objective:
14:   $w_m \leftarrow \mathcal{W}$        ▷ get weights from covariance matrix
15:   $f(n)_+ = w.n^2 \quad \forall w \in w_m, n \in n_m$ 
16: end for


---


17: Step 2: Iterate through components without measurements
   ( $\mathcal{G}$ ) and add terms to the constraint set  $\mathcal{H}$ :
18: for  $j \in \mathcal{G}$  do           ▷ for non-measured grid components
19:    $\mathcal{P}_j \leftarrow \mathcal{P}$          ▷ get params form param set
20:   if  $\exists \mathcal{P}_j \in \mathcal{P}_U$  then
21:      $\mathcal{H} = \mathcal{H} \cup h_j(V, \mathcal{P}_j)$ 
22:   else
23:      $\mathcal{H} = \mathcal{H} \cup h_j(V)$ 
24:   end if
25: end for
26: constraint set  $\mathcal{H}$  is complete with all terms in 1


---


27: Step 3: Solve the optimization to obtain estimates
28:  $\min f(n)$ 
   s.t.  $\mathcal{H}(V, n, \mathcal{P}_U) = 0$ 
29: Output:  $\hat{V}, \hat{\mathcal{P}}_U$ 

```

IV. EXPERIMENT DESIGN

To study the performance of the proposed approaches, we consider several experiments, categorized by 2 setups, which operate on 3 scenarios. The setups are described below:

- **Setup 1 (S1):** Stand-alone estimation of battery (**Bt-SE**), PV (**PV-SE**) and bulk grid system (**ckt-SE**) states
- **Setup 2 (S2):** Combined estimation of battery, PV, and bulk grid system states (**ckt-SE**^{Re} and **ckt-PSE**^{Re})

S1 estimates each component independently following methodology in Section III-C1. **S2** performs combined estimation based on methodology in Section III-C2. We consider

TABLE I: Test Cases Used

Test Case	Network	Number of PV	Number of Battery	Unknown Parameter
TC1	IEEE-118	11	0	No
TC2a	2869pegase	10	2	No
TC2b	2869pegase	10	1	Yes
TC3	ACTIVSg10k	100	0	No

three scenarios to compare the performance of stand-alone setup **S1** against the combined setup **S2**:

- In scenario A, we estimate the system states when all parameters are known, and the measurements only include white noise
- In scenario B, we estimate the system states when all parameters are known, and certain measurements include biased bad data
- In scenario C, we estimate the system states with unbiased noisy measurements but study the estimation robustness against *certain* erroneous parameters

We use 4 test cases to study the three scenarios. The cases are described in Table. I. All test cases are in per unit system with a base of 100 MW. Cases 1 through 4 study scenario A. Case 2 focuses on scenario B, and Case 3 focuses on scenario C. In all experiments, the estimation quality of the grid parameters and states is not the key focus. See prior work in that regard [6].

For each scenario, we ran 100 instances (N_s) with random noise realizations to produce statistically relevant results for estimation with the two setups. We assume all injection nodes are measured on the grid with an RTU, and all solar PV or battery subsystems have measurements available. The choice of measurements is described in Section III-A. To generate synthetic measurements, we first simulate the stand-alone and combined systems and record the simulation solution. Next, we draw noise samples from a zero-mean Gaussian distribution with a standard deviation value of 0.001 [5] for RTU measurements and a deviation value of 0.1 for inverter readings and add those to the simulation results. For scenarios including bad data, we assume that bad data comes from a PV or battery system meter. The bad measurement is assumed to be biased in magnitude and output non-zero mean noise.

Scenario C studies the estimation performance in the presence of erroneous parameters. We induce errors in R_S parameter in the solar PV system. We choose these as erroneous as they are more likely to be incorrect than other parameters: R_S account for interconnection loss, which varies from site to site.

Result metrics: We compare the experiment outcome based on the following error metrics: normalized root mean square error (NRMSE), variance (σ^2), and estimation error (%). The estimation error is how much the estimation differs in percentage compared to the true value; the formula is shown in (40), where \hat{y} and y_{true} represents the estimated value and the true value of the unknown state.

$$\text{Estimation Error}(\%) = \frac{(\hat{y} - y_{true})}{y_{true}} 100 \quad (40)$$

$$RMSE_{\mathbf{y}} = \sqrt{\frac{\sum_{n=1}^{N_s} \sum_{c=1}^{N_c} (\hat{y}_{nc} - y_{true,c})^2}{N_s N_c}} \quad (41)$$

$$NRMSE_{\mathbf{y}} = \frac{RMSE_{\mathbf{y}}}{\hat{y}_{avg}} \quad (42)$$

$$\sigma_c^2 = \frac{\sum_{n=0}^{N_s} (\hat{y}_{nc} - \hat{y}_{avg,c})^2}{N_s} \quad (43)$$

$$\sigma_{avg}^2 = \frac{\sum_{c=1}^{N_c} \sigma_c^2}{N_c} \quad (44)$$

Here \hat{y}_{nc} is the estimate of n^{th} run of component c , which can be PV, battery, or grid node voltage. $\hat{y}_{avg,c}$ is the average value of estimates across the N_s runs of simulations of component c . The NRMSE and variance for grid nodes, battery, or solar PV state and parameter estimates are all calculated in the same manner.

The error can be positive or negative when comparing the battery SoC estimation. Because the error accumulates by time step, we use the absolute error to keep the figure consistent:

$$\text{Absolute Error}(\%) = \left| \frac{(\hat{y} - y_{true})}{y_{true}} 100 \right| \quad (45)$$

V. EXPERIMENT RESULTS

The following section shows state and parameter estimation results in three main scenarios: for test cases with and without bad data in measurements and test cases with erroneous parameters. We compare the performance of stand-alone algorithms against **ckt-SE^{Re}** for the first two scenarios and against **ckt-PSE^{Re}** for the third scenario. We summarize the solving time for various experiments to show that **ckt-SE^{Re}** and **ckt-PSE^{Re}** scales well.

A. State estimation of solar PV and battery system without bad data

Both stand-alone and combined algorithms can estimate the state of the battery and PV system. To compare their performance, we summarize the PV state estimation accuracy for all four test cases in Table II. In TC1, TC2a, TC2b, and TC3, we observe that both stand-alone and **ckt-SE^{Re}** perform well; however, **ckt-SE^{Re}** consistently outperforms stand-alone algorithm. Note that in Table II through Table V, DC power refers to the power injection from the PV system to the inverter and also the DC charging power from the rectifier to the battery, defined by $I_{PV}V_{PV}$ for solar PV and $I_{Bt}V_{Bt}$ for the battery.

TABLE II: PV State estimation results (w/o bad data).

Algo./Case	V_{PV}		V_{SH}		DC Power	
	NRMSE	σ_{avg}^2	NRMSE	σ_{avg}^2	NRMSE	σ_{avg}^2
PV-SE /TC1	2.7E-02	2.5E-02	9.2E-01	8.6E-01	2.6E-01	6.7E-05
ckt-SE^{Re} /TC1	2.6E-01	2.4E-02	8.5E-01	8.0E-01	2.7E-01	6.4E-05
PV-SE /TC2a	2.7E-02	2.5E-02	9.2E-01	8.6E-01	2.7E-02	5.7E-05
ckt-SE^{Re} /TC2a	2.3E-02	2.1E-02	6.7E-01	6.3E-01	2.7E-02	6.4E-05
PV-SE /TC2b	2.6E-02	3.3E-02	8.2E-01	1.5E+00	3.9E-02	1.6E-04
ckt-SE^{Re} /TC2b	1.2E-02	1.3E-02	1.7E-01	1.2E-01	1.9E-02	2.4E-05
PV-SE /TC3	2.8E-02	2.5E-02	9.6E-01	9.0E-01	9.6E-03	6.3E-05
ckt-SE^{Re} /TC3	2.5E-02	2.3E-02	8.0E-01	7.6E-01	9.9E-03	6.7E-05

Fig. 8 plots the DC terminal voltage (V_{PV}) estimation error for *least performant* 10 out of the 100 PV systems in the 10k TC3 network. The **ckt-SE^{Re}** (bottom) observes better estimation accuracy over **PV-SE**, which is prone to high-error outliers. Fig. 9 shows the estimation error (%) for DC terminal voltage (V_{PV}), DC current output (I_{PV}), and DC

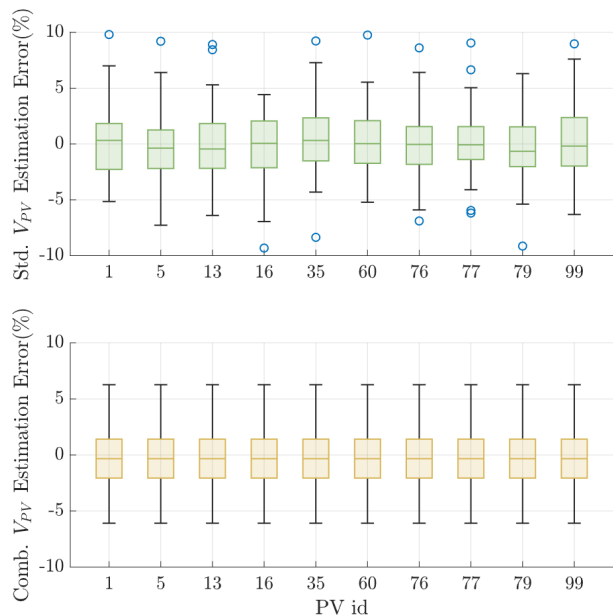


Fig. 8: V_{PV} estimation result of 10k node TC3 network without bad data; this box and whisker plot show V_{PV} estimation result of 10 PV systems with the highest error with the **PV-SE** and **ckt-SE^{Re}**. The **ckt-SE^{Re}** algorithm (Comb.) estimates are less erroneous and more consistent with no outliers than stand-alone (Std.) estimates.

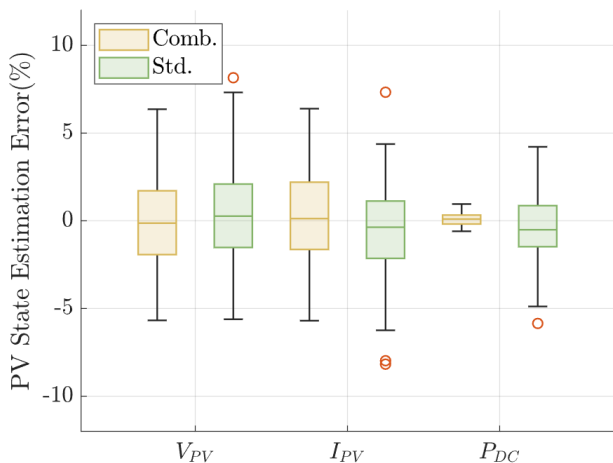


Fig. 9: PV state estimation error w/o bad data on *least accurate* PV system in 2869 node TC2a network. The **PV-SE** (Std.) algorithm performs well but is less accurate and has outliers in comparison to the **ckt-SE^{Re}** (Comb.) algorithm.

power output in 2869 node TC2a. As before, the combined **ckt-SE^{Re}** algorithm performs better than the stand-alone **PV-SE** algorithm as stand-alone estimation tends to have a wider spread across various noise instances and has outliers. We chose this experiment's PV system with the highest power estimation variance.

For battery systems, in Fig. 10, we compare the state of charge estimation absolute error (%) for stand-alone **Bt-SE** and combined **ckt-SE^{Re}** algorithm for two (2) batteries in TC2a network. Table III shows estimation results of the DC terminal, open circuit voltages, and DC power states of the batteries in TC2a. While we observe similar results for DC terminal states, SoC errors for stand-alone **Bt-SE** are far higher

TABLE III: Battery State Estimation Results (w/o bad data)

Algo./Case	V_{Bt}		V_{oc}		DC Power	
	NRMSE	σ_{avg}^2	NRMSE	σ_{avg}^2	NRMSE	σ_{avg}^2
Bt-SE /TC2a	2.6E-03	3.3E-03	3.8E-02	4.1E-04	2.4E-03	7.7E-07
ckt-SE^{Re} /TC2a	2.5E-03	3.0E-03	3.8E-03	4.1E-04	2.3E-03	6.9E-07

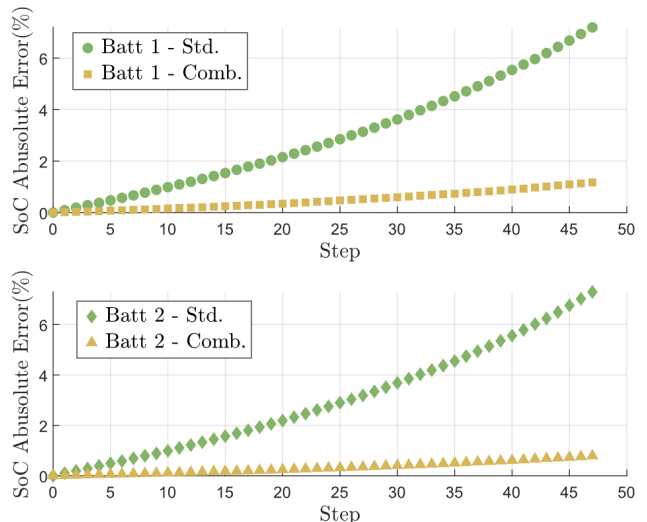


Fig. 10: Absolute errors of SoC estimate for two batteries in TC2a with identical charging and discharging profile and w/o bad-data. Here, each step is 5min, and we simulate a total of 48 steps to represent a 4hr discharging and charging cycle. We observe SoC error accumulates over time and is far worse ($>6\%$ vs. $<2\%$) for the stand-alone **Bt-SE** algorithm.

than combined **ckt-SE^{Re}**, as they accumulate over time.

B. State estimation of solar PV and battery system with bad data

Realistically, not all measurements are free from bad data. Thus, we include bad data points in the next set of Scenario B's experiments. Considering the reliability and cost of different measurement equipment, we placed bad data in solar PV and battery measurements instead of the grid measurements as they have cheaper and less reliable meters without a dedicated communication platform. We use biased V-I measurements to represent an incorrectly calibrated meter. With TC2a network as the test case, we place a +10% error on both $V_{PV,Z}$ and $I_{PV,Z}$ measurements to create bad data, while the RTU measurements contain only white noise. We observe in Fig. 11-12 and Table IV-V that for stand-alone (**PV-SE** and **Bt-SE**) algorithms, estimates deteriorate significantly. However, estimates from the **ckt-SE^{Re}** algorithm are reasonably accurate as they are aided by redundant and accurate RTU measurements from the grid.

C. Parameter State joint estimation

In scenario C, we consider erroneous parameters in estimation experiments. We assume the PV system's R_S parameter is unknown for 1 out of 10 PV systems and run the stand-alone and combined **ckt-PSE^{Re}** algorithm on 2869 node TC2b network. Table VI documents the results. We see that **PV-SE** stand-alone algorithm (with unknown parameters) is less accurate

TABLE IV: PV State Estimation Results (with bad data).

Algo./Case	V_{PV}		V_{SH}		DC Power	
	NRMSE	σ_{avg}^2	NRMSE	σ_{avg}^2	NRMSE	σ_{avg}^2
Bt-SE /TC2a	8.3E-02	5.2E-01	7.3E-02	3.4E-01	7.0E-02	6.0E-04
ckt-SE^{Re} /TC2a	2.6E-02	8.6E-01	2.3E-02	7.7E-01	2.1E-02	1.2E-06

Compared to scenario A w/o bad data, both algorithms in scenario B provide less accurate estimates. However, **ckt-SE^{Re}** is significantly more accurate, as shown in NRMSE results; the variance of V_{SH} and V_{PV} are higher due to the bad data, especially non-zero mean noise.

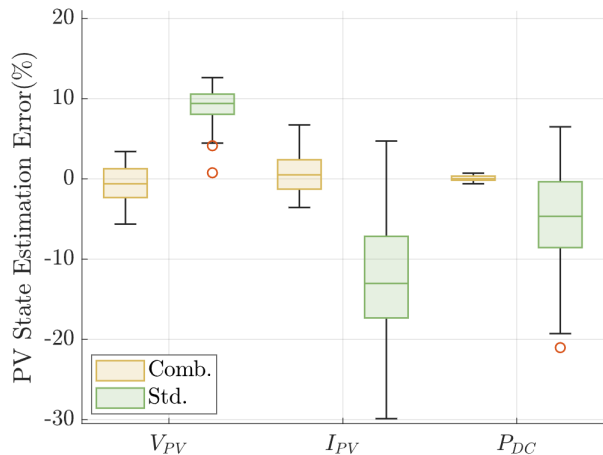


Fig. 11: PV state estimation error with bad data in TC2a. Compared to Fig. 9, the estimation quality deteriorates for both algorithms due to biased voltage current readings. However, **ckt-SE^{Re}** estimates are significantly more accurate than **PV-SE**.

compared to **ckt-PSE^{Re}** by a factor of $\geq 4x$ more error. To visualize the parameter accuracy quality, we build a box plot in Fig. 13. Our first observation is that **ckt-PSE^{Re}** estimation accuracy is significantly better than the stand-alone algorithm. However, in some scenarios, we still observe up to 40% error in parameter estimate. However, note that the median tends to provide a good estimate for the parameter value. Therefore, if we were to obtain recurrent estimates over a certain time window when the parameter can be assumed unchanged, the median value of the parameter estimate can be expected to be accurate.

D. Scalability

Next, we study the scalability of combined **ckt-SE^{Re}** and **ckt-PSE^{Re}** algorithms. The time-complexity of stand-alone algorithms is less critical to discuss as each component is independent and can be estimated in parallel; the bottleneck will always be the largest subsystem; in our case, the largest subsystem is the grid subsystem.

TABLE V: Battery State Estimation Results (with bad data).

Algo./Case	V_{Bt}		V_{OC}		DC Power	
	NRMSE	σ_{avg}^2	NRMSE	σ_{avg}^2	NRMSE	σ_{avg}^2
Bt-SE /TC2a	9.2E-02	9.4E-03	9.2E-02	9.7E-02	1.7E-01	1.0E-06
ckt-SE^{Re} /TC2a	8.6E-02	4.4E-03	8.6E-03	4.8E-01	9.9E-02	7.3E-07

Compared to unbiased Scenario A, both algorithms yield less accurate results. However, **ckt-SE^{Re}** estimates are 1.5x - 8x better than **Bt-SE** per NRMSE numbers.

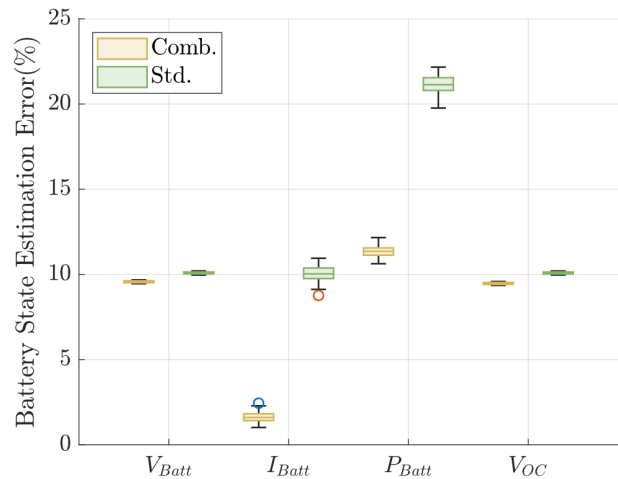


Fig. 12: Battery state estimation error with bad data for 2869 node TC2a network; the x-axis includes various battery states of interest, and the y-axis shows the absolute estimation error. While both algorithms provide biased estimation due to bad data, the **ckt-SE^{Re}** method is more accurate compared to **Bt-SE**.

TABLE VI: Parameter Estimation Accuracy Evaluation

Algo./Case	NRMSE _P	σ_P^2
PV-SE /TC2b	7.1E-01	1.2E-01
ckt-PSE^{Re} /TC2b	1.8E-01	7.4E-03

The time complexity of the combined **ckt-SE^{Re}** algorithm is shown in Fig. 14. The smaller networks with up to 10 PV and battery systems solve in 4 seconds. The largest $>10k$ nodes TC3 network with 40k+ variables and 100 PV systems takes 80 seconds at most. This validates that our approach is scalable and can be implemented in grid control rooms.

VI. CONCLUSION

The paper was inspired by the lack of standard techniques to estimate utility-scale solar PV and battery storage system

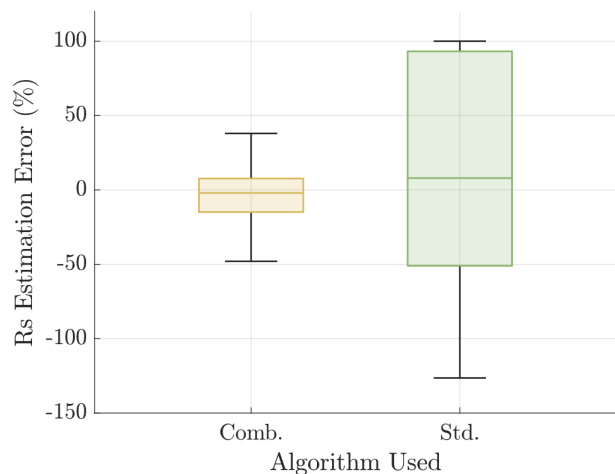


Fig. 13: PV parameter estimation result comparison for TC2b. This box plot shows the parameter estimation results for 100 runs when R_s is unknown. **ckt-PSE^{Re}** provides an interquartile range between -14% to 8% and a median of -2% compared to the stand-alone method with an interquartile range between -93% to 51% and a median of 8%.

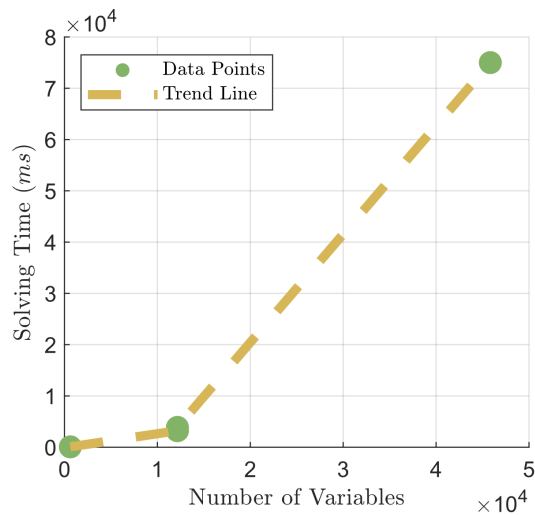


Fig. 14: Runtime for different cases v.s. number of variables in the case. The number on the x-axis shows the number of unknown variables in the optimization problem.

states consistent with transmission system measurements amid the growing number of these systems on the grid. We built a circuit-based joint parameter-state estimation framework **ckt-PSE^{Re}** to accurately model and estimate the states for solar PV, battery storage, and the transmission grid systems within one combined framework. We leveraged circuit models for solar PV, battery storage, and grid components and combined them into one aggregated circuit to perform estimation analysis. We included measurements from all components without loss of generality, and we minimized the measurement noise subject to circuit-based Kirchhoff’s constraints to obtain state estimates. We draw the following conclusions:

- Combined **ckt-SE^{Re}** algorithm outperforms stand-alone algorithms regarding estimation accuracy with or without the existence of bad data; we observe $>3x$ improvement in scenario B for PV systems and $1.5x - 8x$ improvement for battery per standard error metrics
- Combined **ckt-PSE^{Re}** is more robust to erroneous parameters. **ckt-PSE^{Re}** is $3.9x$ more accurate per standard error metric compared to stand-alone algorithms.
- Combined **ckt-PSE^{Re}** algorithm scales and can be used in grid control rooms; we solve the estimation problem for $>10k$ node network with 100 PV systems in about 80 seconds

REFERENCES

- [1] *Short-Term Energy Outlook 2024*. EIA, 2024. URL: https://www.eia.gov/outlooks/steo/pdf/steo_full.pdf.
- [2] Richard Bowers, Elesia Fasching, and Katherine Antonio. *As solar capacity grows, duck curves are getting deeper in California - U.S. energy information administration (EIA)*. June 2023. URL: <https://www.eia.gov/todayinenergy/detail.php?id=56880>.
- [3] Junping Wang et al. “Combined state of charge estimator for electric vehicle battery pack”. In: *Control Engineering Practice* 15.12 (2007), pp. 1569–1576.
- [4] Zhi Fang et al. “State estimation for situational awareness of active distribution system with photovoltaic power plants”. In: *IEEE Transactions on Smart Grid* 12.1 (2020), pp. 239–250.
- [5] Shimiao Li et al. “A circuit-theoretic approach to state estimation”. In: *2020 IEEE PES Innovative Smart Grid Technologies Europe (ISGT-Europe)*. IEEE, 2020, pp. 1126–1130.
- [6] Peng Sang and Amritanshu Pandey. “Circuit-theoretic Joint Parameter-State Estimation–Balancing Optimality and AC Feasibility”. In: *arXiv preprint arXiv:2404.10676* (2024).
- [7] Aleksandar Jovicic et al. “Enhanced modelling framework for equivalent circuit-based power system state estimation”. In: *IEEE Transactions on Power Systems* 35.5 (2020), pp. 3790–3799.
- [8] Min Chen and Gabriel A Rincon-Mora. “Accurate electrical battery model capable of predicting runtime and IV performance”. In: *IEEE transactions on energy conversion* 21.2 (2006), pp. 504–511.
- [9] Yi-Bo Wang et al. “Steady-state model and power flow analysis of grid-connected photovoltaic power system”. In: *2008 IEEE international conference on industrial technology*. IEEE, 2008, pp. 1–6.
- [10] Zhi Fang et al. “Active distribution system state estimation incorporating photovoltaic generation system model”. In: *Electric Power Systems Research* 182 (2020), p. 106247.
- [11] Thomas Easwarakhanthan et al. “Nonlinear minimization algorithm for determining the solar cell parameters with microcomputers”. In: *International journal of solar energy* 4.1 (1986), pp. 1–12.
- [12] Diego Oliva, Erik Cuevas, and Gonzalo Pajares. “Parameter identification of solar cells using artificial bee colony optimization”. In: *Energy* 72 (2014), pp. 93–102.
- [13] MF AlHajri et al. “Optimal extraction of solar cell parameters using pattern search”. In: *Renewable energy* 44 (2012), pp. 238–245.
- [14] Henry Miniguano et al. “General Parameter Identification Procedure and Comparative Study of Li-Ion Battery Models”. In: *IEEE Transactions on Vehicular Technology* 69.1 (2020), pp. 235–245. DOI: 10.1109/TVT.2019.2952970.
- [15] Habiballah Rahimi-Eichi, Federico Baronti, and Mo-Yuen Chow. “Online adaptive parameter identification and state-of-charge coestimation for lithium-polymer

- battery cells”. In: *IEEE Transactions on Industrial Electronics* 61.4 (2013), pp. 2053–2061.
- [16] Mohd Afifi Jusoh and Muhamad Zalani Daud. “Accurate battery model parameter identification using heuristic optimization”. In: *International Journal of Power Electronics and Drive Systems* 11.1 (2020), p. 333.
- [17] David M. Bromberg et al. “An equivalent circuit formulation of the power flow problem with current and voltage state variables”. In: *2015 IEEE Eindhoven PowerTech*. 2015, pp. 1–6. DOI: 10.1109/PTC.2015.7232632.
- [18] Marko Jereminov et al. “Improving robustness and modeling generality for power flow analysis”. In: *2016 IEEE/PES Transmission and Distribution Conference and Exposition (T&D)*. IEEE, 2016, pp. 1–5.
- [19] Amritanshu Pandey et al. “Robust power flow and three-phase power flow analyses”. In: *IEEE Transactions on Power Systems* 34.1 (2018), pp. 616–626.
- [20] Ali M Humada et al. “Solar cell parameters extraction based on single and double-diode models: A review”. In: *Renewable and sustainable energy reviews* 56 (2016), pp. 494–509.
- [21] T Ikegami et al. “Estimation of equivalent circuit parameters of PV module and its application to optimal operation of PV system”. In: *Solar energy materials and solar cells* 67.1-4 (2001), pp. 389–395.
- [22] Maryam Naeijian et al. “Parameter estimation of PV solar cells and modules using Whippy Harris Hawks Optimization Algorithm”. In: *Energy Reports* 7 (2021), pp. 4047–4063.
- [23] Weidong Xiao et al. “Efficient approaches for modeling and simulating photovoltaic power systems”. In: *IEEE journal of photovoltaics* 3.1 (2012), pp. 500–508.
- [24] JA Gow and CD Manning. “Development of a photovoltaic array model for use in power-electronics simulation studies”. In: *IEE Proceedings-Electric Power Applications* 146.2 (1999), pp. 193–200.
- [25] Javier Cubas, Santiago Pindado, and Marta Victoria. “On the analytical approach for modeling photovoltaic systems behavior”. In: *Journal of power sources* 247 (2014), pp. 467–474.
- [26] Paul Gilman. *SAM photovoltaic model technical reference*. Tech. rep. National Renewable Energy Lab.(NREL), Golden, CO (United States), 2015.
- [27] Gilbert M Masters. *Renewable and efficient electric power systems*. John Wiley & Sons, 2013.
- [28] Wenlu Zhou et al. “Review on the battery model and SOC estimation method”. In: *Processes* 9.9 (2021), p. 1685.